Published in final edited form as:
Small. 2011 January 3; 7(1): 126–136. doi:10.1002/smll.201001466.

Oxidative Stress Mediates the Effects of Raman-Active Gold Nanoparticles in Human Cells

Dr. Avnesh S. Thakor,
Molecular Imaging Program at Stanford (MIPS), Department of Radiology, Stanford University, The James H. Clark Center, 318 Campus Drive, Stanford, CA 94305-5427, USA. Department of Radiology, University of Cambridge Cambridge, CB2 2QQ, UK

Dr. Ramasamy Paulmurugan,
Molecular Imaging Program at Stanford (MIPS), Department of Radiology, Stanford University, The James H. Clark Center, 318 Campus Drive, Stanford, CA 94305-5427, USA

Paul Kempen,
Department of Materials Sciences & Engineering, Stanford University CA 94305-5427, USA

Dr. Cristina Zavaleta,
Molecular Imaging Program at Stanford (MIPS), Department of Radiology, Stanford University, The James H. Clark Center, 318 Campus Drive, Stanford, CA 94305-5427, USA

Prof. Robert Sinclair,
Department of Materials Sciences & Engineering, Stanford University CA 94305-5427, USA

Dr. Tarik F. Massoud, and
Molecular Imaging Program at Stanford (MIPS), Department of Radiology, Stanford University, The James H. Clark Center, 318 Campus Drive, Stanford, CA 94305-5427, USA. Department of Radiology, University of Cambridge Cambridge, CB2 2QQ, UK

Prof. Sanjiv S. Gambhir
Molecular Imaging Program at Stanford (MIPS), Department of Radiology, Stanford University, The James H. Clark Center, 318 Campus Drive, Stanford, CA 94305-5427, USA. Department of Materials Sciences & Engineering, Stanford University CA 94305-5427, USA. Department of Bioengineering and Bio-X Program Stanford University CA 94305-5427, USA

Sanjiv S. Gambhir: sgambhir@stanford.edu

Abstract

Polyethylene glycol (PEG)ylated Raman-active gold nanoparticles (PEG-R-AuNPs) consist of an interchangeable Raman organic molecule layer held onto a gold nanocore by a silica shell. PEG-R-AuNPs have been shown preclinically to increase the sensitivity and specificity of Raman spectroscopy, with picomolar sensitivity and multiplexing capabilities. Although clinical trials are being designed to use functionalized PEG-R-AuNPs in various applications (e.g., to target dysplastic bowel lesions during colonoscopy), the effects of these nanoparticles on human cells

Correspondence to: Sanjiv S. Gambhir, sgambhir@stanford.edu.

remain unknown. The occurrence and mechanisms underlying any potential cytotoxicity induced by these nanoparticles (0–1000 PEG-R-AuNPs/cell) are investigated in immortalized human HeLa and HepG2 cell lines at several time points (0–48 h) after exposure. Using fluorometric assays, cell viability (MTT), reactive oxygen species (ROS) generation (dichlorofluoresceindiacetate), protein oxidation (protein carbonyl content), and total cellular antioxidant concentrations the concentrations (metmyoblobin-induced oxidation of ABTS) are assessed. Analysis of lipid oxidation using an enzyme immunoassay (8-isoprostane concentrations), gene expression of antioxidant enzymes using quantitative reverse transcription polymerase chain reactions, and the intracellular location of PEG-R-AuNPs using transmission electron microscopy is also undertaken. PEG-R-AuNPs cause no cytotoxicity in either HeLa or HepG2 cells in the acute setting as ROS generation is balanced by antioxidant enzyme upregulation. Following prolonged exposures (48 h) at relatively high concentrations (1000 PEG-R-AuNPs/cell), nanoparticles are found within vesicles inside cells. Under these conditions, a minimal amount of cytotoxicity is seen in both cell lines owing to increases in cellular oxidative stress, most likely due to ROS overwhelming the antioxidant defenses. Evidence of oxidative stress-induced damage includes increased lipid and protein oxidation. Although further in vivo toxicity studies are necessary, these initial encouraging results show that PEG-R-AuNPs cause minimal toxicity in human cells in the acute setting, which bodes well for potential future applications of these nanoparticles in living subjects.

1. Introduction

In recent years, nanobiotechnology has contributed significantly to developments in the synthesis of new molecular imaging agents and therapeutics. In particular, nanoparticles are now being used preclinically to increase the sensitivity and specificity of various optical imaging techniques.[1,2] These advances have therefore fueled renewed interest in their potential for selected surface-weighted optical imaging applications in future clinical practice. One variety of nanoparticle in particular demonstrates great promise for clinical translation, with picomolar sensitivity and multiplexing capabilities in living animals.[3,4] This nanoparticle consists of a Raman-active organic molecule, with a narrow-band spectral signature, adsorbed onto a 60-nm gold nanocore (Figure 1). This arrangement dramatically increases the incident electromagnetic field of the Raman molecule layer via a phenomenon known as surface-enhanced Raman scattering (SERS), thereby dramatically amplifying its Raman signal intensity. The entire nanoparticle is encapsulated in a silica shell to hold the Raman-active organic molecule on the gold nanocore. The Raman-active gold nanoparticle (R-AuNP) can also be functionalized to allow it to target specific molecular epitopes (Figure 1). The physical and chemical characteristics of this nanoparticle have also been specifically optimized to minimize any potential cellular toxicity. However, studies investigating the effects of R-AuNPs on human cells have yet to be reported and are critically needed, especially since clinical trials involving these R-AuNPs are crucially dependent on such toxicity studies.

Nanoparticles have been shown to possess very different properties compared to their corresponding bulk material. This has significant implications for the use of nanoparticles in vivo since their small size will affect their mode of endocytosis, cellular trafficking, and processing. In addition, their high surface area to volume ratio, surface reactivity, and charge

will dramatically alter their chemical and physical properties resulting in them possessing unexpected toxicities and biological interactions. Although several studies have been undertaken to investigate the toxicity associated with specific classes of nanoparticles, the results are often highly variable.[5–7] This is attributed, in part, to the different shapes, sizes, and chemical preparations of nanoparticles as well as the type of human cell line studied. Nevertheless, there is an increasing body of evidence to now suggest that reactive oxygen species (ROS) play a central role in mediating the toxicity associated with many nanoparticles.[6,8,9]

In healthy aerobic cells, the production of ROS is approximately balanced by antioxidant defense systems. However, an imbalance between pro-oxidant mechanisms and anti-oxidant defenses promotes oxidative stress. It has been suggested that nanoparticles can cause increased cellular oxidative stress by inducing toxic free radical formation in subcellular compartments. As a consequence, cells exposed to oxidative stress can either adapt or become injured. Adaptation usually occurs following exposure to transient levels of oxidative stress, which, in turn, results in an upregulation of antioxidant synthesis or a change in the sensitivity of the cell. Both of these measures will serve to protect the cell against future exposure to oxidative stress. In contrast, cell injury may occur due to oxidative damage to biomolecules if the challenge is too severe or chronic, which results ultimately in cell death. In many situations it is unclear which biomolecule is the most important target, since injury mechanisms overlap widely. However, certain reactive species have preferred targets, such as the hydroxyl radicals targeting DNA[10] and the peroxyl radicals targeting lipid membranes.[11] Oxidation of cellular phospholipids and proteins has been shown to ultimately induce mitochondrial dysfunction, which is thought to be the executioner of cell death.[6]

This study aims to investigate the effects of R-AuNPs on two separate human cell lines. Since all chemicals are inevitably toxic at high doses, it is therefore paramount to investigate the effects of these R-AuNPs at concentrations that are likely to be encountered by cells when used in living subjects, commonly believed to be in the range of 1–100 nanoparticles per cell.[12] As several in vivo biodistribution studies have shown nanoparticles to preferentially accumulate in the liver,[13,14] the HepG2 hepatocyte cell line was chosen. In addition, the HeLa cell line was studied as it represents the traditional cell line used in most human toxicology experiments. In this study R-AuNPs were PEGylated, but not functionalized, to represent the base unit of nanoparticle that would most likely be used in potential future clinical applications. To elucidate the mechanisms responsible for any toxic effects mediated by these PEG-R-AuNPs, biochemical assays were used to measure ROS generation and indices of ROS-induced damage, including tissue phospholipid and protein oxidation, for a range of nanoparticle concentrations and at several different time points. We studied the cellular antioxidant defense mechanisms using an assay that measures the total cellular antioxidant concentration. In addition, we measured the change in gene expression of phase-2 antioxidant enzymes by using quantitative reverse transcription polymerase chain reactions (q-RT-PCRs).[15]

2. Results

2.1. Cell Viability

There were no signs of cytotoxicity in both HeLa and HepG2 cells when incubated with all concentrations of PEG-R-AuNPs for 4 h when compared to untreated control cells (Figure 2). However, following 8 h of incubation, HepG2 cells showed a moderate but significant decrease ($p < 0.05$) in cell viability at high PEG-R-AuNP concentrations (100 and 1000 PEG-R-AuNPs/cell). After 24 h, both HeLa (−23 ± 2%) and HepG2 (−13 ± 4%) cells showed a significant decrease ($p < 0.05$) in cell viability compared to control cells at the highest PEG-R-AuNP concentration (1000 PEG-R-AuNPs/cell). Low concentrations of PEG-R-AuNP had no significant effect ($p > 0.05$) on cell viability in either cell line following 24 h of treatment (Figure 2). By 48 h, cell viability in both cell lines was significantly decreased ($p < 0.05$) following treatment with almost all concentrations of PEG-R-AuNPs. This effect was more pronounced and dose-dependent in HeLa cells (PEG-R-AuNPs/cell 0: −7 ± 3%, 10: −16 ± 6%, 100: −29 ± 5%, 1000: −38 ± 1%; Figure 2).

2.2. Reactive Oxygen Species Production

Following 24 h of incubation, there was a basal increase in ROS production in HeLa (2 h: 489 ± 9 vs 24 h: 1615 ± 49 relative units at 530 nm) and HepG2 (2 h: 534 ± 16 vs 24 h: 2086 ± 54 relative units at 530 nm) cells compared with control cells not receiving any PEG-R-AuNPs (Figure 3). Up to 4 h following treatment with all concentrations of PEG-R-AuNPs, there were no signs of any increase in ROS production in either HeLa or HepG2 cells as compared with the corresponding control cells (Figure 3). After 8 h, all cells treated with PEG-R-AuNPs demonstrated a significant increase ($p < 0.05$) in ROS production compared to control cells (Figure 3). However, there was no additional effect on the amount of ROS produced at the higher doses of PEG-R-AuNP treatment (1000 PEG-R-AuNPs/cell, HeLa: 1099 ± 28; HepG2: 1091 ± 13 relative units at 530 nm) compared to the lower doses (0 PEG-R-AuNPs/cell, HeLa: 1021 ± 22; HepG2: 1075 ± 32 relative units at 530 nm) in either cell line. After 48 h, PEG-R-AuNP-treated cells demonstrated a pronounced increase in ROS production compared to control cells in both cell lines (1000 PEG-R-AuNPs/cell, HeLa: 6501 ± 118; HepG2: 6470 ± 289 relative units at 530 nm). Furthermore, treatment with either 100 or 1000 PEG-R-AuNPs/cell at this time point produced more ROS than cells treated with 1 PEG-R-AuNP/cell (Figure 3). Cells treated with hydrogen peroxide as a positive control demonstrated a profound increase in ROS production at all time points (HeLa 2 h: 1858 ± 38, 48 h: 6809 ± 222; HepG2 2 h: 2537 ± 45, 48 h: 8204 ± 229 relative units at 530 nm).

2.3. Oxidative Stress-Induced Cellular Damage

In HepG2 control cells that received no PEG-R-AuNPs, there was no increase in either tissue phospholipid or protein oxidation up to 48 h. Although HeLa cells also demonstrated no increase in tissue phospholipid oxidation up to 48 h post-exposure, there was a significant increase ($p < 0.05$) in protein oxidation at 48 h (10.3 ± 1.0 pg mL^{-1}) compared to earlier time points (2 h: 4.4 ± 1.2 pg mL^{-1}; Figure 4 and 5). Treatment with all concentrations of PEG-R-AuNPs had no effect on either tissue phospholipid or protein oxidation up to 4 h in either cell line. However, at 8 h there was a significant increase in tissue phospholipid

oxidation at the highest PEG-R-AuNP concentration in both cell lines (1000 vs 0 PEG-R-AuNPs/cell, HeLa: 15.2 ± 4.2 vs 3.8 ± 2.4 pg mL^{-1}; HepG2: 16.3 ± 2.0 vs 5.4 ± 2.5 pg mL^{-1}). Although a similar change was seen when measuring protein oxidation in HepG2 cells at 8 h (10.2 ± 0.8 vs 5.7 ± 1.5 nmol mL^{-1}), there was no increase in protein oxidation for any concentration of PEG-R-AuNPs in HeLa cells (5.0 ± 0.8 vs 4.4 ± 0.4 nmol mL^{-1}; Figure 4 and 5). After 24 h, there was a significant increase ($p < 0.05$) in tissue phospholipid and protein oxidation in both HeLa and HepG2 cells at high PEG-R-AuNP concentrations, with the effect being dose dependent in HeLa cells (48 h PEG-R-AuNPs/cell, 1: 5.9 ± 3.1, 10: 8.1 ± 3.5, 100: 18.1 ± 3.2, 1000: 26.5 ± 5.3 pg mL^{-1}). Interestingly, whilst HepG2 cells seemed to be more sensitive to tissue phospholipid oxidation with significant increases ($p < 0.05$) seen at 10 PEG-R-AuNPs/cell at 24 h and 48 h, HeLa cells seemed to be more sensitive to protein oxidation with significant increases ($p < 0.05$) seen at 1 and 10 PEG-R-AuNPs/cell at 48 h (Figure 4 and 5).

2.4. Antioxidant Defenses

In HepG2 control cells that received no PEG-R-AuNPs, there was no increase in the total cellular antioxidant enzyme concentration up to 48 h (2 h: 0.10 ± 0.03 vs 48 h: 0.25 ± 0.03 mM; Figure 6). In contrast, there was a significant increase in cellular antioxidant enzyme concentration in HeLa cells (2 h: 0.44 ± 0.02 mM) after 4 h (0.55 ± 0.01 mM) and 8 h (0.76 ± 0.01 mM), with no further increase up to 48 h (0.77 ± 0.03 mM). Treatment with PEG-R-AuNPs resulted in an increase in cellular antioxidant enzyme concentrations as early as 2 h in both HeLa and HepG2 cells. Whilst antioxidant enzyme concentrations increased further at 8 and 24 h in HeLa cells in a dose-dependent fashion, no further increase was seen in HepG2 cells. At 48 h, there were significant dose-dependent increases ($p < 0.05$) in antioxidant enzyme concentrations in both cell lines (Figure 6).

Following treatment of both cell lines with 1000 R-AuNPs/cell, gene expressions of four key antioxidant enzymes were determined using q-RT-PCR and compared to control cells which received no PEG-R-AuNPs. HeLa cells demonstrated a significant increase ($p < 0.05$) in catalase (2.3 ± 1.3 fold), superoxide dismutase (1.9 ± 0.5 fold), and hemoxygenase (1.9 ± 0.5 fold) at 48 h when compared to control cells, with catalase gene expression increasing as early as 24 h (Figure 7a). Although glutathione peroxidase gene expression had a tendency to increase at later time points, none of the changes in gene expression for this enzyme achieved statistical significance (Figure 7a). Interestingly, HepG2 cells demonstrated a significant increase in catalase (2.5 ± 0.3 fold), superoxide dismutase (1.7 ± 0.1 fold), hemoxygenase (2.6 ± 0.3 fold), and glutathione peroxidase (1.7 ± 0.3 fold) slightly earlier at 24 h when compared to control cells (Figure 7b), with both catalase and hemoxygenase demonstrating increased gene expression at 8 h (Figure 7b). The results were normalized with β-actin.

2.5. Subcellular Location of the R-AuNPs

For both HeLa and HepG2 cells, no nanoparticles were observed inside the cells at the low concentration of 1 R-AuNP/cell following 48 h of treatment. In contrast, nanoparticles were found within vesicles inside both cell lines at the high concentration of 1000 R-AuNPs/cell

following 48 h of treatment (Figure 8). Fewer nanoparticles were observed within the vesicles inside HeLa cells compared to HepG2 cells (Figure 8).

3. Discussion

Our results show that treatment with PEG-R-AuNPs in the acute setting causes no cytotoxicity at concentrations between 0 and 1000 PEG-R-AuNPs/cell in either HeLa or HepG2 cells. However, some cytotoxicity is seen in both cell lines, mainly at higher nanoparticle concentrations, after prolonged continuous exposure to PEG-R-AuNPs. One mechanism that may account for this cytotoxicity is an increase in cellular oxidative stress. In support of this hypothesis, we have demonstrated an increase in ROS generation in both the cells lines studied following prolonged PEG-R-AuNP exposure. At the relatively early time points, there are increases in antioxidant enzyme concentrations in both cell lines, which appear to balance any deleterious effects associated with ROS, thereby protecting the cell. Although the antioxidant enzyme concentrations continue to increase over time, the amount of ROS produced most likely overwhelms these antioxidant defenses since both cell lines demonstrate evidence of oxidative stress-induced damage with increased tissue phospholipid and protein oxidation. This damage could therefore account for the limited cytotoxicity associated with PEG-R-AuNPs at the later time points and higher concentrations.

The PEG-R-AuNPs used in our experiments have a complex structure consisting of a gold nanocore, a Raman-active layer, a silica shell, and surface-attached PEG molecules (Figure 1). This arrangement allows the phenomenon known as SERS to amplify the inelastic light scattering signal from the Raman-active layer, which, in turn, enables increased sensitivity for signal detection. As the Raman-active layer can be changed, this enables the potential for in vivo multiplexing of signal production since each nanoparticle will carry its own signature, thereby enabling it to be detected independently. Indeed, multiplexing with these nanoparticles has recently been demonstrated in vivo by our laboratory using five spectrally unique SERS nanoparticles.[3] The silica shell is an inert material that encloses the molecule, thereby keeping the Raman-active layer tightly applied to the gold nanocore whilst guaranteeing physical robustness, insensitivity to environmental conditions, and provision of a simple surface for biofunctionalization. Previous studies examining silica nanoparticles in living animals have shown their biological inertness, with only an acute inflammatory response seen at 12 h post-exposure and no further treatment-related response seen up to 4 weeks thereafter.[16] Moreover, silica nanoparticles are efficiently cleared from the body via urine, bile, and feces, with any nanoparticles remaining within the body harmlessly residing within the macrophages of the reticuloendothelial system.[16] Finally, as “naked” nanoparticles adsorb proteins that make them aggregate, this renders them unsuitable for applications in cell biology since they are thus relatively unstable in biological media/serum. Hence, our nanoparticles were coated with PEG, which serves as a biological layer to improve stability, water solubility, and biocompatibility and reduce potential protein adsorption and aggregation.[17,18] Moreover, PEG chains also allow the nanoparticles to be functionalized by serving as linking conduits that provide a terminal group for the conjugation of ligands that can target specific molecular epitopes in vivo.

In general, the toxicity induced by nanoparticles depends on their physical and chemical characteristics which, in turn, determine the mechanism and efficiency of how they enter and leave a cell, in addition to how they are processed and metabolized once inside a cell.[19,20] Recently, it has been shown that the physical size of nanoparticles is probably the most important criterion when considering nanomaterial toxicity. Spherical nanoparticles, like our PEG-R-AuNPs, have been shown to be less toxic than other nanoparticle shapes[21] and appear to enter cells via receptor-mediated endocytosis.[22] This process depends on two factors: 1) the thermodynamic force for membrane wrapping, which refers to the amount of free energy required for a membrane to enclose a nanoparticle and drive it into a cell; and 2) the receptor diffusion kinetics, which refers to the recruitment of receptors to the nanoparticle binding site.[19] Although nanoparticles can be taken up into cells nonspecifically, functionalized nanoparticles will depend heavily on the receptor diffusion kinetics of the target cell. Mathematical modeling of the mechanisms of receptor-mediated endocytosis,[23] together with experimental studies examining the size dependence of nanoparticles,[19,24,25] have shown that the most efficient cellular uptake of nanoparticles occurs within the size range of 25–50 nm. However, particles with positive surface charges could interact strongly with a negatively charged cell membrane such that these charge interactions would push the optimal wrapping size to larger particles. Nevertheless, nanoparticles larger than 50 nm, such as our PEG-R-AuNP which measures approximately 120 nm in diameter, will have a slower wrapping time due to slower receptor diffusion kinetics, since more receptors will be taken up during the binding process leaving fewer available for any subsequent nanoparticle binding. Hence, the size of our PEG-R-AuNP is optimal for it to function as a molecular imaging probe that can gain access to cell membrane receptors whilst also being large enough to prevent efficient receptor-mediated endocytosis, thereby minimizing any potential toxicity it could cause by entering cells.

For any nanoparticle that manages to enter a cell, its physical size again determines how it is processed. Typically, smaller nanoparticles are able to enter the nucleus through nuclear pores and irreversibly bind to and damage DNA.[18] In addition, small AuNPs (1.4 nm) have also been shown to cause cytoplasmic disorganization, nuclear fragmentation, and membrane blebbing in HeLa cells.[26] In contrast, larger nanoparticles will usually remain trapped within vesicles away from organelles, thereby limiting their ability to cause damage and cytotoxicity.[27,28] Our TEM results support these findings and demonstrate only small numbers of PEG-R-AuNPs located within endocytic vesicles inside cells after 48 h. Although more PEG-R-AuNPs were found within HepG2 cells compared to HeLa cells, this was possibly due to the intrinsic phagocytic nature of this cell line resulting in a more efficient receptor-mediated endocytosis. Furthermore, only minimal cytotoxicity was seen with our PEG-R-AuNP after 48 h, unlike previous studies which have demonstrated significant cytotoxicity when using smaller nanoparticles.[20,26] However, caution is necessary when comparing results from different nanoparticle studies since the actual number of nanoparticles to which cells are exposed cannot be accurately determined from standard units of concentrations due to differences in nanoparticle sizes, shapes, compositions, and functionalizations, all of which affect the molecular weight of the particle being studied. Although no PEG-R-AuNPs were seen in the cytoplasm, our study was only conducted foro 48 h to minimize the effects of nutrient depletion or cellular overgrowth in

our experimental cell culture wells. In addition, as TEM sections are 60–80 nm thick, they only represent a fraction of the entire cell volume and hence it is plausible that some PEG-R-AuNPs could be present within a cell but not be detected if they were not present within a selected slice. Nevertheless, as our PEG-R-AuNPs are larger than 74 nm, if they did manage to enter cells they were likely to remain inside the cell for longer. Evidence for this is derived from experiments which have shown that as the size of the AuNPs increases, their rate of exocytosis from cells dramatically decreases with 74-nm nanoparticles leaving cells twice as slowly compared to 14-nm nanoparticles.[19] Further study is therefore necessary to determine the long-term effects of the presence of these PEG-R-AuNPs within cells. Nevertheless, the large size of each R-AuNP would mean that even if they do escape from the vesicles and enter into cytoplasm, their physical size would most likely hinder both their access to the nucleus (diameter of the nuclear pore complex in HeLa cells is about 39 nm[29]) and their interaction with DNA.

In addition to physically interacting with various components within a cell, several studies have shown nanoparticles to increase the generation of intracellular ROS[8,30–32] through the oxidative burst phenomenon and through interference with the mitochondrial electron-transport chain.[33] In agreement with this, the present data demonstrate an increase in ROS production in both cell lines tested following exposure to PEG-R-AuNPs. Interestingly, the control cells, which were not treated with nanoparticles, showed a small but significant increase in ROS production over 48 h. This may be attributed to cells being stressed due to either the depletion of nutrients from the unchanged media or the competition for physical space within each well as cells continue to divide. Nevertheless, the cells that were treated with PEG-R-AuNPs showed significantly increased ROS generation compared to the control cells at each time point. In general, an increase in ROS production is normally balanced by cells increasing their antioxidant defense capacity. However, when the production of ROS overwhelms the antioxidant defenses, the cell enters a state of oxidative stress where ROS can cause damage to the cell either directly via the oxidation of cellular protein and phospholipids or indirectly through the activation of a number of redox-signaling cascades.

Recently, Xiao and colleagues proposed a hierarchical oxidative stress model consisting of three tiers, which cells employ in response to nanoparticle-sized material.[15] In brief, at low levels of oxidative stress (Tier 1), cells employ protective effects via the induction of the transcription factor, nuclear factor erythroid 2-related factor 2 (Nrf2), which leads to the transcriptional activation of >200 antioxidant and detoxification enzymes that are collectively known as the phase 2 response.[34,35] The phase 2 enzymes include anti-oxidants such as hemoxygenase. glutathione-*S*-transferase, catalase, superoxide dismutase, and glutathione peroxidase, which prevent adverse biological outcome from nanoparticle-induced ROS production. However, should these responses fail to provide adequate protection, any further increase in ROS production can result in proinflammatory (Tier 2) and cytotoxic (Tier 3) effects.[8] Whilst the proinflammatory effects have been shown to be mediated by redox-sensitive mitogen-activated protein (MAP) kinase and nuclear factor NF-κB cascades, the cytotoxic effects usually involve the mitochondria, which are capable of releasing proapoptotic factors and inducing apoptosis. Our results show that although R-AuNPs induced the generation of ROS, they also induced a Tier 1 response in cells, which

resulted in the activation of phase-2 antioxidant defenses. This is supported by an increase in the total antioxidant enzyme concentration in both cell lines together with q-RT-PCR, thus demonstrating an upregulation of catalase, superoxide dismutase, haemoxygenase, and glutathione peroxidase. Interestingly, whilst both cell lines demonstrated a similar-fold increase in gene expression of phase-2 antioxidant enzymes, HepG2 cell gene expression peaked at 24 h following PEG-R-AuNP treatment whereas HeLa cells demonstrated a steady increase over 48 h. This earlier increase in HepG2 cells may be explained by these cells having an intrinsically lower basal antioxidant capacity, as demonstrated by their lower total antioxidant enzyme concentration than HeLa cells. Since R-AuNP treatment appeared to generate similar levels of ROS in both cell lines, HepG2 cells would therefore need to upregulate their anti-oxidant enzymes sooner to prevent an increase in oxidative stress. Although the total antioxidant enzyme concentration increased in both cell lines as early as 4 h following R-AuNP treatment, no further significant increase was seen up to 48 h later, except at the highest R-AuNP concentration in HepG2 cells. However, the production of ROS continued to increase, thereby resulting in cells suffering an increase in oxidative stress at later time points as demonstrated by increases in protein and phospholipid oxidation. This increase in cellular oxidative stress in both cell lines appears to be directly correlated with a Tier 3 response in both cells, equivalent to an increase in cytotoxicity. This effect was more pronounced at the higher PEG-R-AuNP concentrations and at the later time points. Since the Tier 3 response to nanoparticles has been shown to involve mitochondrial injury,[32] we therefore chose the MTT (3-(4,5-dimethylthiazol-2-yl)-2,5-diphenyltetrazolium bromide) assay to measure cellular cytotoxicity; this assay relies on viable mitochondria to cleave the tetrazolium ring in the MTT solution. By demonstrating cellular cytotoxicity, this assay also indirectly provides evidence that this was due to mitochondrial injury.

While the results from this cell culture study are encouraging, caution should be exercised in the immediate extrapolation to the human setting and how PEG-R-AuNPs might be processed in living subjects. As the present studies were carried out on immortalized human cells, by definition these cells will therefore be more resistant to cell death and hence our results may actually underestimate the overall toxicity of these PEG-R-AuNPs. Although minimal cytotoxicity was observed in the acute setting, studies of longer duration may be necessary to examine the fate of these PEG-R-AuNPs. As the PEG-R-AuNPs are made of several different components (i.e., PEG molecules, silicon layer, Raman organic molecule, and gold nanocore), the overall integrity of the nanoparticles over time will need to be closely scrutinized to determine whether they remain intact or whether they are broken down by cells into their individual constituents. In a cell culture setting, an artificial environment is also created in which cells are exposed to high numbers of static nanoparticles, an effect that is unlikely to occur in living subjects due to the dynamic nature of the circulation which distributes nanoparticles throughout the body. Furthermore, at any given location in the body there are likely to be multiple cell types that interact with each other creating an integrated response to PEG-R-AuNPs. Although we now understand how hepatocytes react to PEG-R-AuNPs, this is unlikely to be a realistic representation of the in vivo response within a living subject's liver owing to the wide variety of different cell types that make up this organ. Indeed, in addition to hepatocytes the liver also contains macrophages (otherwise known as Kupffer cells) and sinusoidal endothelial cells, which have both been shown to be

very active in clearing and eliminating nanoparticles in living animals.[36,37] Finally, as PEG-R-AuNPs will eventually be functionalized with different molecular tags depending on the clinical scenario to allow them to target different molecular epitopes, this may alter how cells perceive, interact with, and process these nanoparticles. Accordingly, further studies in living subjects are now required to investigate the toxicity of PEG-R-AuNPs and functionalized PEG-R-AuNPs, with particular attention being paid to the effects on specific organs that may be targeted during diagnosis and treatment, for example the bowel, if clinical translation using these nanoparticles to detect dysplastic mucosal lesions at colonoscopy is to be considered in future human clinical trials.

4. Experimental Section

Nanoparticle Characteristics

R-AuNPs were obtained from Oxonica Materials Inc. (Mountain View, CA, USA) and consisted of a 60-nm gold nanocore, a Raman-active organic molecule, and a 30-nm silica shell, thus making the entire nanoparticle on the order of 120 nm in diameter (Figure 1). The particular lot used in this study was the S440 batch, which consisted of a unique Raman-active material layer (*trans*-1,2-bis(4-pyridyl)ethylene); its associated spectrum can be seen in our previous work.[3] Two different-sized PEG molecules, Mal-PEG_{2000}-OME and Mal-PEG_{5000}-NHS, were added to the surface of the R-AuNP in a 5:1 ratio, respectively. The smaller Mal-PEG_{2000}-OME was added to improve nanoparticle biocompatibility while the larger Mal-PEG_{5000}-NHS was added to provide a functional group for potential ligand attachment. Both surface-PEG chains were added to the surface of these nanoparticles in a two-step process. Initially, thiol groups were introduced into the silica shell of the nanoparticle using 3-mercaptopropyltrimethoxysilane. This was followed by conjugation with malemide-activated mPEGs, where the malemide group reacted with the thiol group on the nanoparticle surface at neutral pH. To ensure consistency between the experiments, all PEG-R-AuNPs were created at the same time from the same batch of stock nanoparticles received from Oxonica Materials Inc. All nanoparticles were stored at 4 °C between experiments.

Cell Preparation

Pathogen-free HeLa and HepG2 cell lines (American Type Culture Collection) were grown in a 75 cm^2 flask in Dulbecco's Minimal Essential Medium (DMEM) supplemented with 10% fetal bovine serum (FBS), 1% penicillin and streptomycin, and 1 mM sodium pyruvate, in a fully humidified incubator containing 5% CO_2 at 37 °C. The cell culture medium was replenished every two days and cells passaged once they reached 80% confluence.

Experimental Preparation

Depending on the experimental protocol, either 30 000 cells (for a 96-well plate) or 250 000 cells (for a six-well plate) were added to each well of an experimental plate in sterile DMEM and left at 37 °C for at least 8 h for stabilization prior to the addition of PEG-R-AuNPs. The exact number of cells that were plated was determined using an automated cell counter (Invitrogen). Since the concentration of the stock solution of nanoparticles provided by Oxonica Materials Inc. was 0.8 nM, using Avogadro's constant (6.022×10^{23} elementary

entities per mole of substance) we determined that there were 481 760 000 PEG-R-AuNPs per microliter of stock solution. Hence, by using serial dilutions of the stock solution, final concentrations of 0, 1, 10, 100, and 1000 PEG-R-AuNPs could then be achieved. All nanoparticle preparations were suspended in sterile DMEM and vortexed for 20 s to minimize agglomeration before being added to the cell culture medium in each well. The experimental plate was then gently swirled to uniformly distribute the nanoparticles amongst the plated cells. Following exposure to PEG-R-AuNPs, cells were left for either 2, 4, 8, 24, or 48 h in a fully humidified incubator containing 5% CO_2 at 37 °C before being subjected to one of the assays detailed below. For each assay, separate experiments were performed for each PEG-R-AuNP concentration at every time point. As a small proportion of cells were inevitably lost during either the collection or washing procedures involved in each assay, the results were normalized based on each sample's protein concentration as determined by the Bradford Assay.[38] The protein concentration directly relates to the number of cells present in each sample being analyzed. All experimental assays were performed in at least triplicate, unless otherwise stated, with results expressed as the mean ± SEM. Comparisons between time (2, 4, 8, 24, and 48 h) and dose (0, 1, 10, 100, and 1000 PEG-R-AuNPs/cell) were assessed statistically using two-way ANOVA with repeated measures (RM; Sigma-Stat; SPSS Inc., Chicago, IL, USA). Where a significant effect of time or group was indicated, the post hoc Student–Newman–Keuls test was used to isolate the statistical differences. For all comparisons, statistical significance was accepted when $P < 0.05$.

Assessment of Cell Viability

Cell viability was assessed using the MTT assay (Invitrogen) in which water-soluble MTT is taken up by viable cells and converted to an insoluble formazan. The formazan is then solubilized and the concentration determined spectrophotometrically, with the absorbance directly relating to the number of viable cells present. All experiments were performed in a 96-well plate. At the end of each time point, MTT solution (10 μL, 12 mM) was added to individual wells. For a negative control, MTT solution (10 μL, 12 mM) was added to a well containing DMEM alone (100 μL). Experimental plates were then covered and left to incubate at 37 °C for 4 h. Next, dimethyl sulfoxide (50 μL, to dissolve the formazan) was added to each well and the plates were left at 37 °C for a further 10 min before the absorbance was measured at 540 nm using a microplate spectrophotometer system.

Assessment of ROS Generation

To measure ROS, a fluorometric assay using dichlorofluorescein diacetate (DCFH-DA; Sigma–Aldrich) was performed. DCFH-DA is a cell-permeable non-fluorescent probe which is hydrolyzed by intracellular esterases, thereby trapping it within the cell. This nonfluorescent molecule can then be oxidized by ROS, which turns it into fluorescent dichlorofluorescin (DCF). The level of intracellular fluorescence is therefore proportional to the amount of intracellular ROS generation with a linear dynamic range.[39] DCFH-DA cannot be appreciably oxidized to a fluorescent state without being first hydrolyzed. All experiments were performed in a 96-well plate. Prior to the addition of PEG-R-AuNPs, cells were treated with DCFH-DA (40 μM) and left for 1 h before the start of any experiments. Hydrogen peroxide, which is known to oxidize DCFH-DA, was used as a positive control in

both cell lines. At each time point, the fluorescence from DCF was measured using a microplate spectrophotometer system with excitation and emission wavelengths of 485 and 530 nm, respectively.

Assessment of Lipid Oxidation

One marker that has been widely used to represent the random oxidation of tissue phospholipids by ROS is 8-isoprostane. The concentration of 8-isoprostane in samples can be determined using an enzyme immunoassay (EIA; Cayman Chemical), which relies on the competition between 8-isoprostane and 8-isoprostane–acetylcholinesterase conjugate (a tracer) for a limited number of 8-isoprostane-specific rabbit antiserum binding sites. As the concentration of tracer is held constant while the concentration of 8-isoprostane in samples varies, the amount tracer that binds to the rabbit antiserum is therefore inversely proportional to the concentration of 8-isoprostane present in each well.[40] Quantification of the tracer is achieved by measuring the acetylcholinesterase with Ellman's Reagent, which consists of acetylthiocholine and 5,5′-dithio-bis(2-nitrobenzoic acid). The hydrolysis of acetylthiocholine by acetylcholinesterase produces thiocholine, which can then react with 5,5′-dithio-bis(2-nitrobenzoic acid) to produce 5-thio-2-nitrobenzoic acid, which has a strong absorbance around 415 nm. The EIA plate was obtained from Cayman Chemical and set up as instructed using the cell culture medium (DMEM) for dilution of the 8-isoprostane standards, the nonspecific binding and B_0 wells. All experiments were initially performed in a six-well plate. From each experiment, the culture medium was collected and 50 μL added to each well, together with 50 μL of the tracer and 50 μL of EIA antiserum. Each plate was then covered and left to incubate for 18 h at 4 °C. All wells were then rinsed five times with wash buffer before freshly constituted Ellman's Reagent (200 μL) was added to each well. The absorbance of each sample was measured using a microplate spectrophotometer system at 415 nm. By using the 8-isoprostane standards, a four-parameter logistic equation was used to fit the data and determine the concentration of 8-isoprostane in each sample.

Assessment of Protein Oxidation

Measurement of the protein carbonyl content in samples has been used as a marker of the amount of protein that has been oxidized by highly reactive free radicals. Protein carbonyl content can be quantified using 2,4-dinitrophenylhyrazine (DNPH; Cayman Chemical), which reacts with protein carbonyls to produce the corresponding hydrazone that can be analyzed spectrophotometrically. All experiments were performed in a six-well plate. Cells from each time point were harvested from wells using a rubber policeman. Following centrifugation at 1000 *g* for 10 min, the cell pellet was transferred to ice-cold buffer (2 mL, 50 mM 2-(*N*-morpholino)ethanesulfonic acid at pH 6.7 with 1 mM EDTA) and lysed by sonication. Samples were then centrifuged at 10 000 *g* for 15 min and the supernatant collected for analysis. The absorbance of the supernatant was checked at 280 and 260 nm to ensure the 280/260 ratio was <1, thereby confirming no nucleic acid contamination. For each sample, 200 μL was added to either 800 μL DNPH (experiment tube) or 2.5 M HCl (control tube). Both tubes were incubated in the dark for 1 h at room temperature, being briefly vortexed every 15 min, before being transferred to ice where 20% trichloroacetic acid (TCA; 1 mL) was added. Following 5 min of incubation, the samples were centrifuged at 10 000 *g* for 10 min at 4 °C. The supernatant was then discarded and the pellet

resuspended in 10% TCA (1 mL). Following another 5 min of incubation, the samples were centrifuged at 10 000 *g* for 10 min at 4 °C. The supernatant was again discarded and the pellet resuspended in ethanol/ethyl acetate (1:1, 1 mL) before being centrifuged. This step was repeated twice. After the final wash, the protein pellets were resuspended in guanidine hydrochloride (500 μL) and vortexed thoroughly before being finally centrifuged at 10 000 *g* for 10 min at 4 °C. The absorbance of each sample was measured using a microplate spectrophotometer system at 360 nm. The corrected absorbance was then calculated by subtracting the absorbance of the control sample from the absorbance of the experiment sample. The final protein carbonyl concentration (nmol mL^{-1}) was calculated by dividing the corrected absorbance by the extinction coefficient of DNPH (0.011 μM cm^{-1}). As this was the final experimental assay performed in our study, we only had a limited amount of PEG-R-AuNPs remaining that had been synthesized from the same batch of stock nanoparticles. Hence, these experiments were only performed in duplicate.

Assessment of Total Cellular Antioxidant Concentration

The cooperation of all different antioxidants has been suggested to provide greater protection against ROS than any single compound alone. This assay therefore relies on the ability of antioxidants to inhibit the metmyoglobin-induced oxidation of 2,2′-azino-di-(3-ethylbenzthiazoline sulfonate) (ABTS, Cayman Chemical). All experiments were performed in a six-well plate. Cells from each time point were harvested from wells using a rubber policeman. Following centrifugation at 1000 *g* for 10 min, the cell pellet was transferred to ice-cold buffer (2 mL, 5 mM potassium phosphate at pH 7.4 with 0.9% sodium chloride and 0.1% glucose) and lysed by sonication. Samples were then centrifuged at 10 000 *g* for 15 min and the supernatant collected for analysis. For each sample, 10 μL was added to metmyoglobin (10 μL) and ABTS (150 μL). The oxidation reaction was then triggered by adding hydrogen peroxide (40 μL). Following 5 min of incubation at room temperature, the absorbance of each sample was measured using a microplate spectrophotometer system at 750 nm. All samples were then compared to Trolox (water-soluble tocopherol) standards to estimate their relative antioxidant capacity.

Assessment of Antioxidant Enzyme Gene Expression Using q-RT-PCR

The change in antioxidant gene expression was evaluated for cells treated with 1000 PEG-R-AuNPs/cell and compared with control cells treated with 0 PEG-R-AuNPs/cell at all time points according to methods previously described.[41] All experiments were performed in a six-well plate. At the end of each experiment, total ribonucleic acid (RNA) was extracted from cells using an RNeasy Plus Mini Kit (Qiagen), which contained gDNA eliminator spin columns to effectively remove genomic DNA. The RNA concentration in each sample was then calculated using the Qbit system (Invitrogen). Using RNA (1 μg), complementary DNA (cDNA) was synthesized using reverse transcription (RT) by incubating samples at 25 °C for 5 min followed by 42 °C for 45 min with qScript cDNA Supermix (Quanta Biosciences), which contained buffer, dNTPs, $MgCl_2$, random primers, RNase inhibitor, and reverse transcriptase. RT quantitative polymerase chain reactions (q-RT-PCRs) were then undertaken using the Realplex Mastercycler machine (Eppendorf) with PerfeCTa SYBR Green FastMix, which contained AccuFast Taq DNA polymerase (Quanta Biosciences). All samples were run in triplicate in a 20-μL reaction volume using cDNA of 100 ng RNA

equivalent with an initial preheating phase of 95 °C for 2 min, followed by 60 cycles consisting of 95 °C for 30 s, 55 °C for 30 s, and 68 °C for 30 s. Melting curve analysis was performed for each reaction to exclude nonspecific PCR side products. The primer sequences for four antioxidant enzyme genes (catalase, super-oxide dismutase, hemoxygenase, and glutathione peroxidase) along with the internal control (β-actin) are shown in Table 1.

TEM of Cell Samples

To determine the subcellular location of the PEG-R-AuNPs, both HeLa and HepG2 cells were treated with 1 and 1000 PEG-R-AuNPs/cell in a six-well plate. After 48 h, cells were harvested using a rubber policeman and centrifuged at 1000 *g* for 10 min before being transferred to a 2:1:1 solution of 0.2 M sodium cacodylate buffer/10% glutaraldehyde/8% paraformaldehye (EMSdiasum). Samples were then stored at 4 °C before being stained en bloc with osmium tetroxide. After 2 h, samples were rinsed with deionized water and stained with uranyl acetate overnight. Samples were then dehydrated in progressively higher concentrations of ethanol: 50, 70, 95, and 100%. Samples were further dehydrated using propylene oxide and embedded in Embed 812 epoxy resin (EMSdiasum). Thin sections (150 nm) were then cut using a Leica Ultracut S microtome and placed on a 200-mesh bare copper grid. The sections were examined using a Tecnai G2 X-Twin (FEI) transmission electron microscope operating at 120 kV. Between 200 and 600 cell sections were examined for each of the four samples analyzed.

Acknowledgments

This work was supported in large part by the NCI Center for Cancer Nanotechnology Excellence (CCNE) U54 CA119367 (S.S.G.), NCI Network for Translational Research (NTR): Optical Imaging in Multimodality Platforms (S.S.G.), the NCI In Vivo Cellular and Molecular Imaging Centers (ICMIC) P50 CA114747 (S.S.G.), the Canary Foundation (S.S.G.), the American Cancer Society (A.S.T.), the European Association for Cancer Research (A.S.T.), the PEEL Medical Research Trust (A.S.T.), and NIHR Cambridge Biomedical Research Centre (A.S.T. and T.F.M.). We would also like to thank Ian Walton at Oxonica Inc. for helpful advice.

References

1. Texier I, Josser V. Methods Mol Biol. 2009; 544:393–406. [PubMed: 19488714]
2. Shim SY, Lim DK, Nam JM. Nanomedicine. 2008; 3:215–232. [PubMed: 18373427]
3. Zavaleta CL, Smith BR, Walton I, Doering W, Davis G, Shojaei B, Natan MJ, Gambhir SS. Proc Natl Acad Sci USA. 2009; 106:13511–13516. [PubMed: 19666578]
4. Keren S, Zavaleta C, Cheng Z, de la Zerda A, Gheysens O, Gambhir SS. Proc Natl Acad Sci USA. 2008; 105:5844–5849. [PubMed: 18378895]
5. Brandenberger C, Rothen-Rutishauser B, Muhlfeld C, Schmid O, Ferron GA, Maier KL, Gehr P, Lenz AG. Toxicol Appl Pharmacol. 2009; 242:56–65. [PubMed: 19796648]
6. Pan Y, Neuss S, Leifert A, Fischler M, Wen F, Simon U, Schmid G, Brandau W, Jahnen-Dechent W. Small. 2007; 3:1941–1949. [PubMed: 17963284]
7. Goodman CM, McCusker CD, Yilmaz T, Rotello VM. Bioconjugate Chem. 2004; 15:897–900.
8. Li N, Nel AE. Antioxid Redox Signal. 2006; 8:88–98. [PubMed: 16487041]
9. Park EJ, Park K. Toxicol Lett. 2009; 184:18–25. [PubMed: 19022359]
10. Cadet J, Delatour T, Douki T, Gasparutto D, Pouget JP, Ravanat JL, Sauvaigo S. Mutat Res. 1999; 424:9–21. [PubMed: 10064846]
11. Yoshida Y, Ito N, Shimakawa S, Niki E. Biochem Biophys Res Commun. 2003; 305:747–753. [PubMed: 12763056]

12. Boisselier E, Astruc D. Chem Soc Rev. 2009; 38:1759–1782. [PubMed: 19587967]
13. Schipper ML, Iyer G, Koh AL, Cheng Z, Ebenstein Y, Aharoni A, Keren S, Bentolila LA, Li J, Rao J, Chen X, Banin U, Wu AM, Sinclair R, Weiss S, Gambhir SS. Small. 2009; 5:126–134. [PubMed: 19051182]
14. Sonavane G, Tomoda K, Makino K. Colloids Surf B Biointerfaces. 2008; 66:274–280. [PubMed: 18722754]
15. Xiao GG, Wang M, Li N, Loo JA, Nel AE. J Biol Chem. 2003; 278:50781–50790. [PubMed: 14522998]
16. Cho M, Cho WS, Choi M, Kim SJ, Han BS, Kim SH, Kim HO, Sheen YY, Jeong J. Toxicol Lett. 2009; 189:177–183. [PubMed: 19397964]
17. Prencipe G, Tabakman SM, Welsher K, Liu Z, Goodwin AP, Zhang L, Henry J, Dai H. J Am Chem Soc. 2009; 131:4783–4787. [PubMed: 19173646]
18. Gu YJ, Cheng J, Lin CC, Lam YW, Cheng SH, Wong WT. Toxicol Appl Pharmacol. 2009; 237:196–204. [PubMed: 19328820]
19. Chithrani BD, Chan WC. Nano Lett. 2007; 7:1542–1550. [PubMed: 17465586]
20. Lewinski N, Colvin V, Drezek R. Small. 2008; 4:26–49. [PubMed: 18165959]
21. Wang S, Lu W, Tomvmachenko O, Rai US, Yu H, Ray PC. Chem Phys Lett. 2008; 463:145–149. [PubMed: 24068836]
22. Shi W, Wang J, Fan X, Gao H. Phys Rev E: Stat, Nonlin, Soft Matter Phys. 2008; 78:061914. [PubMed: 19256875]
23. Gao H, Shi W, Freund LB. Proc Natl Acad Sci USA. 2005; 102:9469–9474. [PubMed: 15972807]
24. Chithrani BD, Ghazani AA, Chan WC. Nano Lett. 2006; 6:662–668. [PubMed: 16608261]
25. Jiang W, Kim BY, Rutka JT, Chan WC. Nat Nanotechnol. 2008; 3:145–150. [PubMed: 18654486]
26. Pan Y, Leifert A, Ruau D, Neuss S, Bornemann J, Schmid G, Brandau W, Simon U, Jahnen-Dechent W. Small. 2009; 5:2067–2076. [PubMed: 19642089]
27. Khan JA, Pillai B, Das TK, Singh Y, Maiti S. Chem Bio Chem. 2007; 8:1237–1240.
28. Connor EE, Mwamuka J, Gole A, Murphy CJ, Wyatt MD. Small. 2005; 1:325–327. [PubMed: 17193451]
29. Andersen JS, Lyon CE, Fox AH, Leung AK, Lam YW, Steen H, Mann M, Lamond AI. Curr Biol. 2002; 12:1–11. [PubMed: 11790298]
30. Moller P, Jacobsen NR, Folkmann JK, Danielsen PH, Mikkelsen L, Hemmingsen JG, Vesterdal LK, Forchhammer L, Wallin H, Loft S. Free Radical Res. 2009; 44:1–46. [PubMed: 19886744]
31. Xia T, Kovochich M, Nel A. Clin Occup Environ Med. 2006; 5:817–836. [PubMed: 17110294]
32. Xia T, Kovochich M, Brant J, Hotze M, Sempf J, Oberley T, Sioutas C, Yeh JI, Wiesner MR, Nel AE. Nano Lett. 2006; 6:1794–1807. [PubMed: 16895376]
33. Long TC, Saleh N, Tilton RD, Lowry GV, Veronesi B. Environ Sci Technol. 2006; 40:4346–4352. [PubMed: 16903269]
34. Cho HY, Reddy SP, Kleeberger SR. Antioxid Redox Signal. 2006; 8:76–87. [PubMed: 16487040]
35. Li N, Xia T, Nel AE. Free Radical Biol Med. 2008; 44:1689–1699. [PubMed: 18313407]
36. Sadauskas E, Danscher G, Stoltenberg M, Vogel U, Larsen A, Wallin H. Nanomedicine. 2009; 5:162. [PubMed: 19217434]
37. Briley-Saebo K, Bjørnerud A, Grant D, Ahlstrom H, Berg T, Kindberg GM. Cell Tissue Res. 2004; 316:315. [PubMed: 15103550]
38. Lovrien R, Matulis D. Curr Protoc Microbiol. 2005 Appendix 3A.
39. Wang H, Joseph JA. Free Radical Biol Med. 1999; 27:612–616. [PubMed: 10490282]
40. Pradelles P, Grassi J, Maclouf J. Anal Chem. 1985; 57:1170–1173. [PubMed: 3898913]
41. Pfaffl MW. Nucleic Acids Res. 2001; 29:e45. [PubMed: 11328886]

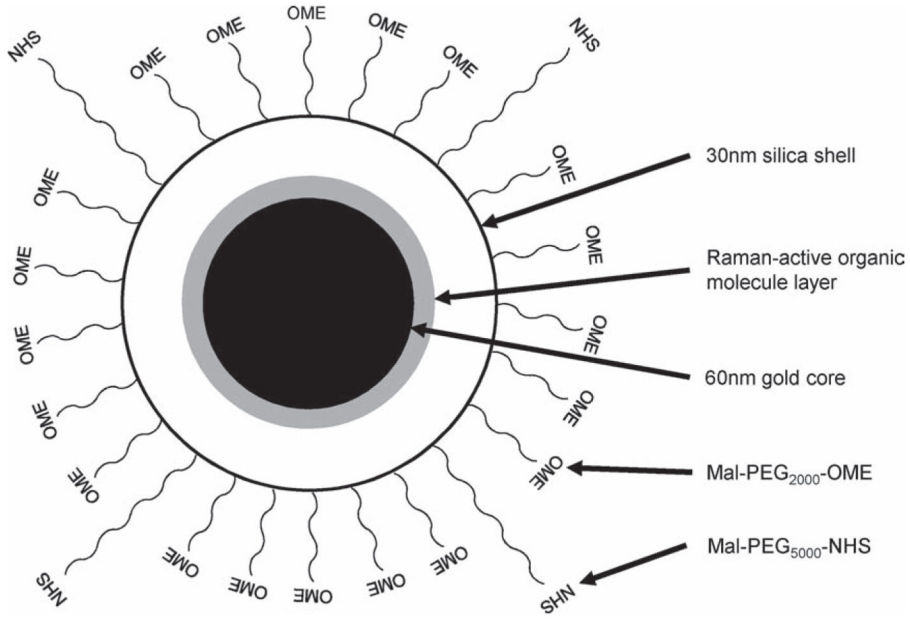

Figure 1.

Diagrammatic representation of the PEGylated R-AuNP (PEG-R-AuNP, PEG = polyethylene glycol). Mal = maleimide, OME = methoxy group.

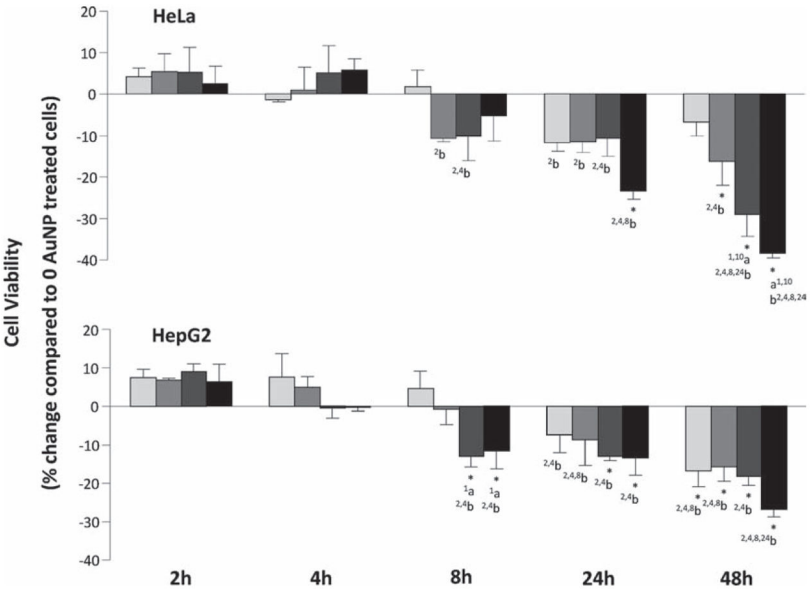

Figure 2.

PEG-R-AuNP-induced inhibition of HeLa and HepG2 cellular proliferation. Bars represent the mean ± standard error of the mean (SEM) for the percentage change in cell viability compared to control cells at 2, 4, 8, 24, and 48 h following incubation with 1 ( ), 10 ( ), 100 ( ), and 1000 (■) PEG-R-AuNPs/cell. Significant differences: **P* < 0.05, difference from own baseline; [a]*P* < 0.05, difference between doses within a time point; [b]*P* < 0.05, difference between time points within a dose. Superscript numbers represent the statistically significant groups (two-way RM ANOVA with post hoc Student–Newman–Keuls test).

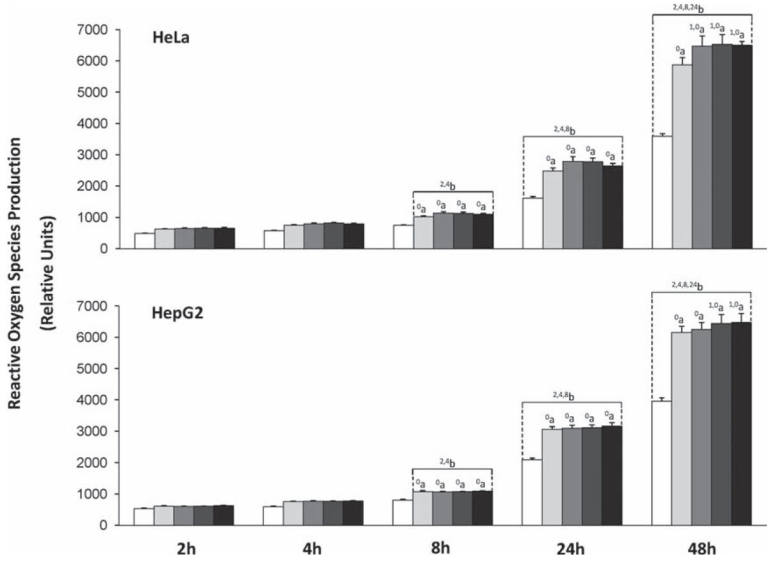

Figure 3.

PEG-R-AuNP-induced changes in reactive oxygen species production in HeLa and HepG2 cells. Bars represent the mean ± SEM for the amount of reactive oxygen species produced at 2, 4, 8, 24, and 48 h following incubation with 0 (□), 1 ( ), 10 ( ), 100 ( ), and 1000 (■) PEG-R-AuNPs/cell. Significant differences: $^{a}P < 0.05$, difference between doses within a time point; $^{b}P < 0.05$, difference between time points within a dose. Superscript numbers represent the statistically significant groups (two-way RM ANOVA with post hoc Student–Newman–Keuls test).

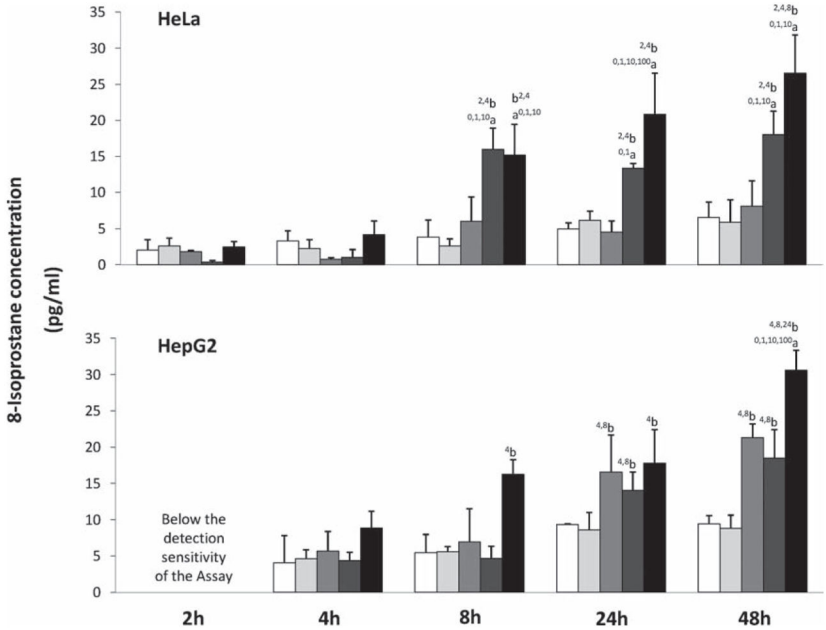

Figure 4.

PEG-R-AuNP-induced changes in tissue phospholipid oxidation in HeLa and HepG2 cells. Bars represent the mean ± SEM for the amount of 8-isoprostane produced at 2, 4, 8, 24, and 48 h following incubation with 0 (□), 1 ( ), 10 ( ), 100 ( ), and 1000 (■) PEG-R-AuNPs/cell. Significant differences: $^{a}P < 0.05$, difference between doses within a time point; $^{b}P < 0.05$, difference between time points within a dose. Superscript numbers represent the statistically significant groups (two-way RM ANOVA with post hoc Student–Newman–Keuls test).

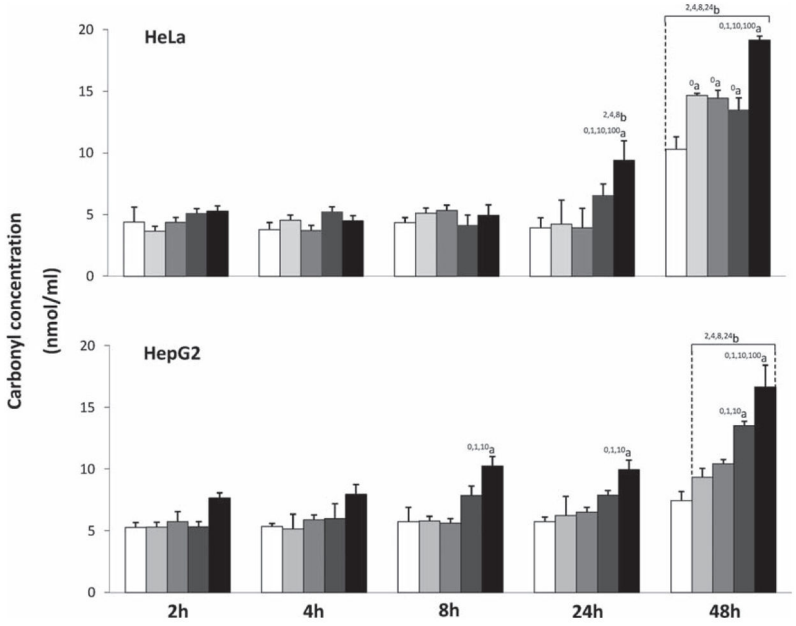

Figure 5.

PEG-R-AuNP-induced changes in protein oxidation in HeLa and Hep G2 cells. Bars represent the mean ± SEM for the amount of carbonyl produced at 2, 4, 8, 24, and 48 h following incubation with 0 (□), 1 ( ), 10 ( ), 100 ( ), and 1000 (■) PEG-R-AuNPs/cell. Significant differences: $^{a}P < 0.05$, difference between doses within a time point; $^{b}P < 0.05$, difference between time points within a dose. Superscript numbers represent the statistically significant groups (two-way RM ANOVA with post hoc Student–Newman–Keuls test).

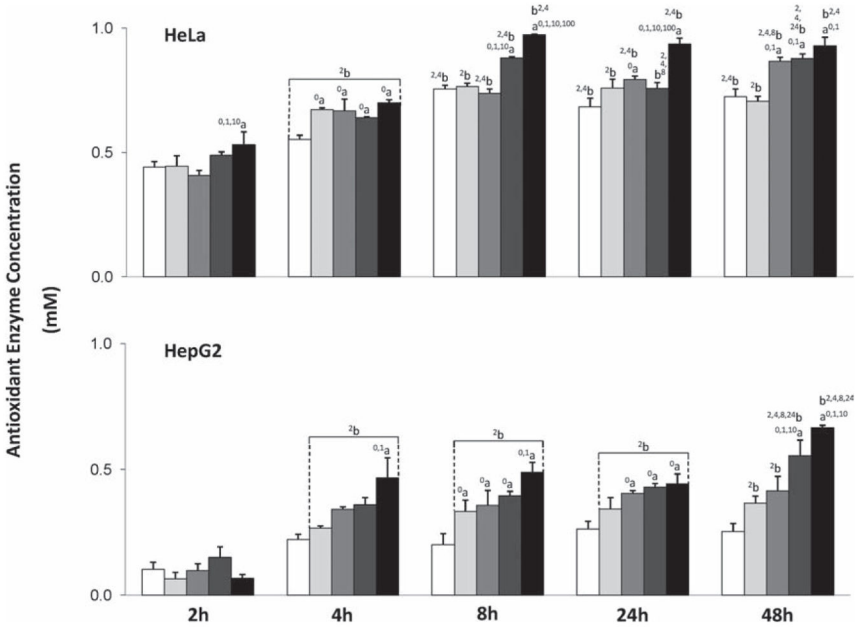

Figure 6.

PEG-R-AuNP-induced changes in antioxidant enzyme concentration in HeLa and HepG2 cells. Bars represent the mean ± SEM for the total amount of antioxidant enzymes produced at 2, 4, 8, 24, and 48 h following incubation with 0 (□), 1 ( ), 10 ( ), 100 ( ), and 1000 (■) PEG-R-AuNPs/cell. Significant differences: $^{a}P < 0.05$, difference between doses within a time point; $^{b}P < 0.05$, difference between time points within a dose. Superscript numbers represent the statistically significant groups (two-way RM ANOVA with post hoc Student–Newman–Keuls test).

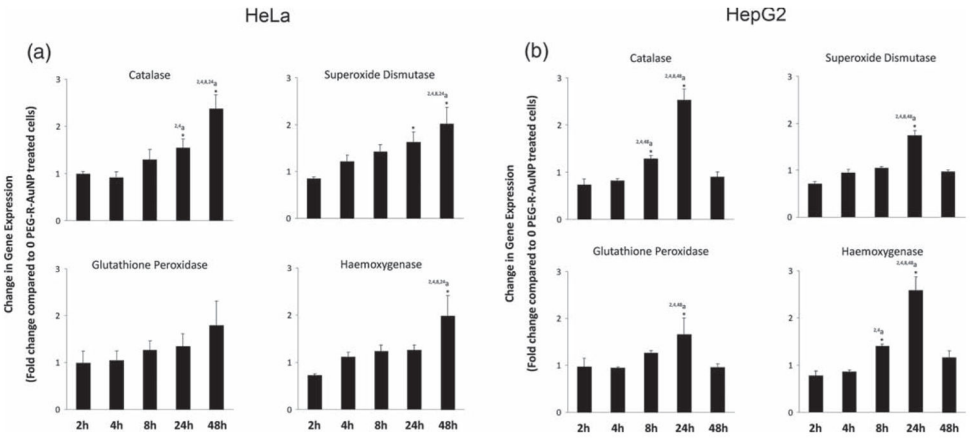

Figure 7.

PEG-R-AuNP-induced change in antioxidant enzyme gene expression in a) HeLa and b) HepG2 cells. Bars represent the mean ± SEM for the fold change in antioxidant enzyme gene expression (mRNA level) compared to control cells at 2, 4, 8, 24, and 48 h following incubation with 1000 PEG-R-AuNPs/cell (■). Significant differences: $*P < 0.05$, difference from control cells treated with 0 PEG-R-AuNPs/cell; $^{a}P < 0.05$, difference between time points. Superscript numbers represent the statistically significant time-point groups (two-way RM ANOVA with post hoc Student–Newman–Keuls test).

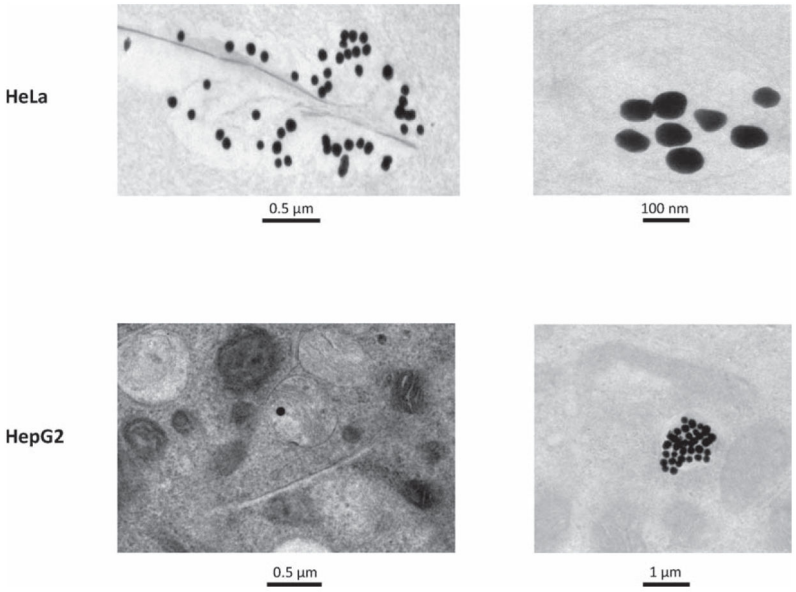

Figure 8.

Transmission electron microscopy (TEM) of HeLa and HepG2 cells treated with 1000 PEG-R-AuNPs/cell for 48 h. PEG-R-AuNPs are shown on the top left in a grouping on the exterior surface and on the top right in a vesicle inside a HeLa cell. PEG-R-AuNPs are also shown within vesicles inside the HepG2 cell line on the bottom left and right.

Table 1

Primer sequences of antioxidant enzyme genes.

Gene name	Primer sequence
catalase	F: 5′-TCATGACATTTAATCAGGCA-3′ R: 5′-GTGTCAGGATAGGCAAAAAG-3′
superoxide dismutase	F: 5′-GAAGGTGTGGGGAAGCATTA-3′ R: 5′-ACATTGCCCAAGTCTCCAAC-3′
glutathione peroxidase	F: 5′-CTCTTCGAGAAGTGCGAGGT-3′ R: 5′-TCGATGTCAATGGTCTGGAA-3′
hemoxygenase-1	F: 5′-CTCTGAAGTTTAGGCCATTG-3′ R: 5′-AGTTGCTGTAGGGCTTTATG-3′
3-actin	F: 5′-GGCGGACTATGACTTAGTTG-3′ R: 5′-AAACAACAATGTGCAATCAA-3′